Int. J. Electrochem. Sci., 15 **(2020)** 8928 – 8942, doi: 10.20964/2020.09.65

International Journal of
ELECTROCHEMICAL
SCIENCE
www.electrochemsci.org

Hydrogen Evolution Inorganic Inhibitors in Alkaline Electrolyte for Aluminum-Air Battery

Seok-Ryul Choi[§], *Sol-Ji Song*[§], *Jung-Gu Kim*[*]

Department of Materials Science and Engineering, Sungkyunkwan University, 2066, Seobu-Ro, Jangan-Gu, Suwon-Si, Republic of Korea, 16419
[§]S.-R. Choi and S.-J. Song contributed equally to this work
[*]E-mail: kimjg@skku.edu

Received: 14 April 2020 / *Accepted:* 3 July 2020 / *Published:* 10 August 2020

Arsenic oxide (As(Ⅲ)), sodium phosphate monobasic anhydrous ($H_2PO_4^-$), and antimony trioxide (Sb(Ⅲ)) are used as electrolyte additives in 4M sodium hydroxide (NaOH) electrolyte for Al-air batteries. The effects of inorganic additives are examined through hydrogen evolution and self-corrosion testing, electrochemical analysis, and surface analysis. Electrochemical tests show that the presence of the additives lowers the hydrogen gas evolution rate and inhibits the adsorption of hydrogen on the aluminum surface. The additives in order of effectiveness are: Sb(Ⅲ) > As(Ⅲ) > $H_2PO_4^-$. The addition of additives decreases the self-corrosion of 4N Al, which improves the efficiency of the Al-air battery. The additives are confirmed as effective inhibitors of the hydrogen generation reaction in Al-air batteries.

Keywords: Aluminum-air battery · Hydrogen evolution · Inhibitor · Battery efficiency · Electrochemical test

1. INTRODUCTION

Aluminum-air batteries have a high potential for electric vehicles or cogeneration plants because of their high energy density (8,100 Wh/kg), low density (2.71 g/cm^3), environmental friendliness and low cost [1-9]. The aluminum-air batteries basically consist of three parts: an aluminum electrode, an air electrode, and an electrolyte. Alkaline solutions are commonly used for electrolytes because they can effectively remove the passive film on the aluminum surface, which degrades battery performance [10-12]. However, when alkaline electrolytes are used, undesirable self-corrosion occurs on the aluminum surface, resulting in a problem of lowering the coulombic efficiency [13-14]. To solve this problem, aluminum alloys are being developed as electrode materials which increase the hydrogen overpotential to suppress the corrosion rate. Inorganic or organic additives are

added to the electrolyte for lower cost and high corrosion inhibition [15-21]. Although most of the additives effectively reduce the rate of corrosion, they also have the problem of inhibiting the aluminum dissolution reaction, which is a power generation reaction. It is an important issue of aluminum-air batteries to suppress the hydrogen production reaction which is the corrosion reaction on the aluminum surface while maintaining the aluminum dissolution reaction.

In this study, we found inorganic additives to improve the performance of aluminum-air cells by reducing corrosion and maintaining power generation reactions. For this, we evaluated the performance of Al-air battery in the presence of arsenic (As(Ⅲ)), phosphorous ($H_2PO_4^-$), and antimony (Sb(Ⅲ)) as electrolyte additives in 4M NaOH electrolyte. These inorganic additives act as substances that inhibit the corrosion reaction by participating in the hydrogen gas formation reaction. The potentiodynamic polarization test was performed in the half cell assembly to evaluate the effect of additives in anodic and cathodic reactions of Al electrode. Hydrogen evolution, self-corrosion, open-circuit potential, and discharge efficiency tests were investigated in the full cell assembly. In addition, surface analysis was conducted to verify the mechanism of the additives.

2. EXPERIMENTAL METHODS

2.1. Specimen and electrolyte

High purity 4N grade (99.99%) Al was used as the anode electrode (Norsk Hydro, Germany). The cathode air diffusion electrode consisted of a nickel (Ni) foam / carbon (C) mixture that contained cobalt oxide (CoO_3) as a catalyst (Meet Inc., Korea). For all experiments conducted in this study, the surface of Al samples and C mixture layer with CoO_3, which contacts the electrolyte, were cleaned with ethanol and distilled water, and then dried with nitrogen (N_2) gas.

4M NaOH electrolyte in distilled water was used as a control electrolyte. To confirm the effects of the additives, three experimental group electrolytes were prepared by adding 10 mM of As(Ⅲ), $H_2PO_4^-$, and Sb(Ⅲ) to 4M NaOH electrolyte. Their respective sources were arsenic oxide (As_2O_3), sodium phosphate monobasic anhydrous (NaH_2PO_4), and antimony trioxide (Sb_2O_3). The four electrolytes used in this study were designated as follows: 4M NaOH, 4M NaOH + 10 mM As(Ⅲ), 4M NaOH + 10 mM $H_2PO_4^-$, and 4M NaOH + 10 mM Sb(Ⅲ) electrolytes.

2.2. Hydrogen evolution test

The 4N Al samples with surface area controlled to Φ15 mm were immersed in each of the four electrolytes for two hours. The hydrogen was collected using a water substitution method that consisted of a measuring cylinder and gas guide tube. The measuring cylinder contained distilled water and the reduction in the volume of water was measured. The hydrogen gas evolution rate, R_{H_2} (mL cm^{-2} min^{-1}) was determined using the following equation:

$$R_{H_2} = V_{H_2}/(A \times T) \quad (1)$$

where V_{H_2} is the volume of the collected hydrogen gas (mL), A is the sample area (cm^2), and T is the immersion time (min).

2.3 Electrochemical measurement

At room temperature, the multi-potentiostat / galvanostat VSP-300 was used to test potentiodynamic polarization and electrochemical impedance spectroscopy (EIS) consisting of a typical three-electrode system. As the reference and counter electrodes, a saturated calomel electrode (SCE) and two pure graphite rods were used. The working electrode was prepared using 4N Al and its surface area was controlled at 1.0 cm^2. The open-circuit potential (OCP) established within 1 h before electrochemical testing was conducted in the four electrolytes. The potentiodynamic tests were carried out in the anodic and the cathodic polarization tests in the ranges of 0 V_{OCP} to 1.0 V_{SCE} and 0 V_{OCP} to -0.5 V_{SCE}, respectively with a scan rate of 0.166 mV s^{-1}. The EIS analysis was performed with an amplitude of ±20 mV at frequencies ranging from 100 kHz to 100 mHz.

2.4. Self-corrosion

Self-corrosion tests of the samples were performed in 4M NaOH, 4M NaOH + 10 mM As(Ⅲ), 4M NaOH + 10 mM $H_2PO_4^-$, and 4M NaOH + 10 mM Sb(Ⅲ) for 2 h using hydrogen collection to estimate the corrosion rate of the 4N Al anode. The weights of the samples before and after immersion were measured following sample cleaning by distilled water and ethanol.

The corrosion rate is calculated by the following equation [22]:

$$\text{Corrosion rate } (mm/year) = 87.6 \times W/D \times A \times T \quad (2)$$

where W is the weight loss (mg), D is the density (g cm^{-3}), A is the sample area (cm^2), and T is the immersion time (hour). The proportionality constant, 87.6, is the conversion factor for W, D, A, and T.

2.5. Battery performance test

Discharge performance of an Al-air battery was evaluated with a constant-current discharge test. The 4N Al and air diffusion electrodes were used as the anode and cathode, respectively. The discharge current density of 10 mA cm^{-2} was applied for 2 h. The discharge efficiency of the anode was calculated by the amount of charge generated and weight lost by the anode. To confirm the effects of additives on each electrode during discharge, a three-electrode cell was constructed. The potentials of the 4N Al and air diffusion electrodes were respectively measured through the same reference electrode in the electrochemical experiment.

2.6. Surface analysis

Surface analysis was conducted by scanning electron microscopy (SEM) to confirm the effects of additives on the 4N Al surface. 4N Al samples were prepared for surface analysis by immersion in the four electrolytes for one hour and were then rinsed with ethanol and distilled water.

3. RESULTS AND DISCUSSION

3.1. Hydrogen evolution and self-corrosion test

Table 1 represents the hydrogen gas evolution rate of 4N Al in 4M NaOH, 4M NaOH + 10 mM As(Ⅲ), 4M NaOH + 10 mM $H_2PO_4^-$, and 4M NaOH + 10 mM Sb(Ⅲ) electrolytes. The hydrogen evolution rate increased in the following order: 4M NaOH + 10 mM Sb(Ⅲ) < 4M NaOH + 10 mM As(Ⅲ) < 4M NaOH + 10 mM $H_2PO_4^-$ < 4M NaOH. The addition of As(Ⅲ) or Sb(Ⅲ) to the 4M NaOH electrolyte decreased the hydrogen gas evolution rate significantly. The addition of $H_2PO_4^-$ slightly reduced the hydrogen evolution rate, but not significantly.

Table 1. Hydrogen gas evolution rates of 4N Al in four electrolytes

Solution	Hydrogen gas evolution rate (mL cm^{-2} min^{-1})
4M NaOH	0.255
4M NaOH + 10 mM As(Ⅲ)	0.127
4M NaOH + 10 mM $H_2PO_4^-$	0.245
4M NaOH + 10 mM Sb(Ⅲ)	0.109

The parasitic hydrogen evolution reaction on the Al surface is as follows [10]:

$$Al + 3H_2O \rightarrow Al(OH)_3 + (3/2)H_2 \quad (3)$$

Because this hydrogen evolution reaction causes the self-corrosion of Al in the electrolyte, the decreased hydrogen generation reaction contributes the reduction of self-corrosion. The self-corrosion rate of 4N Al in the four different electrolytes is represented in Table 2. The self-corrosion rate follows the same tendency as the hydrogen evolution rate: the slower was the hydrogen evolution rate, the slower was the self-corrosion rate of the 4N Al.

Table 2. Corrosion rates of 4N Al from 2 h immersion test in four electrolytes

Solution	Weight loss (mg)	Corrosion rate (mm $year^{-1}$)
4M NaOH	41.4	380.2
4M NaOH + 10 mM As(Ⅲ)	25.7	236.0
4M NaOH + 10 mM $H_2PO_4^-$	40.1	368.3
4M NaOH + 10 mM Sb(Ⅲ)	20.8	191.0

The hydrogen evolution reaction (HER) in alkaline solution proceeds as shown in the following equations 4-6.

$$Volmer: H_2O + e^- \rightarrow H_{ad} + OH^- \quad (4)$$

$$Tafel: 2H_{ad} \rightarrow H_2\,(gas) \quad (5)$$

$$Heyrovsky: H_{ad} + H_2O + e^- \rightarrow OH^- + H_2\,(gas) \quad (6)$$

In the first step, according to the Volmer equation (4), water receives a single electron, forming an intermediate, adsorbed hydrogen (H_{ad}), on the aluminum surface. And then, the adsorbed hydrogen is converted into the hydrogen gas following the process of either the Tafel equation (5) or the Heyrovsky equation (6). In order to generate hydrogen gas, the Volmer equation (4) is inevitably preceded. If this reaction is slowed down, it has an effect on the suppression of the hydrogen evolution reaction. The elements X (As(Ⅲ) and Sb(Ⅲ) of group VA) react with strong chemisoprtion on the aluminum surface called poisoning. Through the following reaction, the strong chemisorption atoms react with adsorbed hydrogens (H_{ad}) on the aluminum surface to form an intermediate phase.

$$X + 3H_{ad} \rightarrow XH_3 \quad (7)$$

Since this reaction is involved in the reaction rate of the Volmer equation (4), it suppresses the hydrogen evolution reaction.

3.2. Electrochemical characteristic test

The effects of the additives can be described either as reducing hydrogen evolution or reducing self-corrosion of Al. That is, it is necessary to confirm whether the reduction in hydrogen evolution is due to the reduction of self-corrosion or the reduction in self-corrosion is due to the reduction of hydrogen evolution. Thus, electrochemical tests were conducted in the four electrolytes.

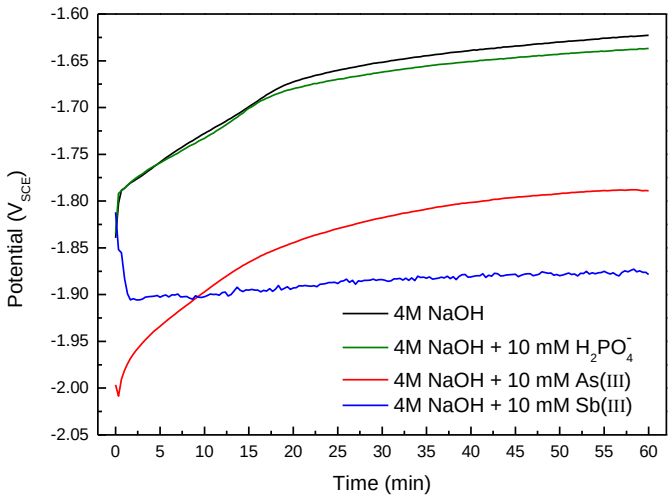

Figure 1. Open-circuit potential vs time for 4N Al in 4M NaOH, 4M NaOH + 10 mM As(Ⅲ), 4M NaOH + 10 mM $H_2PO_4^-$, and 4M NaOH + 10 mM Sb(Ⅲ) electrolytes.

Figure 1 shows the variation of the open-circuit potential (OCP) of 4N Al with time in 4M NaOH electrolyte containing different additives. The $H_2PO_4^-$ and As(Ⅲ) additive curves show similar tendencies to the 4M NaOH curve, that is, their OCPs increase and show a tendency toward saturation

with time. This positive shift in OCP indicates anode passivation resulting from the formation of insoluble oxide or hydroxide of Al [23]. Although the difference of OCP values between 4M NaOH and 4M NaOH + 10 mM $H_2PO_4^-$ electrolytes was not marked, a significant difference appeared between the 4M NaOH and 4M NaOH + 10 mM As(Ⅲ) electrolytes. The addition of As(Ⅲ) in 4M NaOH negatively shifted the OCP and caused an increase in the Al-air battery cell voltage. The addition of Sb(Ⅲ) in 4M NaOH created a significantly different OCP tendency, in that it reached a steady state after an initial sharp decrease in potential. Also, Sb-containing electrolyte showed the most negative shift among the four electrolytes.

The results of potentiodynamic polarization tests are represented in Figure 2. To obtain information about kinetics of corrosion, electrochemical parameters were calculated from the polarization curve: corrosion potential (E_{corr}), corrosion current density (i_{corr}), anodic Tafel slope (β_a), and cathodic Tafel slope (β_c). The corrosion rates of 4N Al in the four different electrolytes were calculated by potentiodynamic polarization test. The corrosion current density obtained by the Tafel extrapolation method can be used to calculate the corrosion rate by Faraday's law [24]:

$$\text{Corrosion rate } (mm/year) = (3.16 \times 10^2 \times i_{corr} \times M)/(zF\rho) \quad (8)$$

where M is the molar mass of the metal (g mol^{-1}), z is the number of electrons transferred per metal atom, F is the Faraday's constant, and ρ is the density of the metal (g cm^{-3}). The polarization data including corrosion rate are listed in Table 3. The addition of additives shifted the corrosion potential (E_{corr}) to negative values similar to the shift OCP, indicating that the additives increases electrochemical activity of 4N Al [25]. The decreases in corrosion current density and corrosion rate of 4N Al increase in the following order: 4M NaOH + 10 mM Sb(Ⅲ) < 4M NaOH + 10 mM As(Ⅲ) < 4M NaOH + 10 mM $H_2PO_4^-$ < 4M NaOH. In alkaline solutions, the corrosion of Al is considered to occur according to the following reactions [26,27]:

$$\text{Al(ss)} + OH^- \rightarrow Al(OH)_{ads} + e^- \quad (9)$$

$$Al(OH)_{ads} + OH^- \rightarrow Al(OH)_{2,ads} + e^- \quad (10)$$

$$Al(OH)_{2,ads} + OH^- \rightarrow Al(OH)_{3,ads} + e^- \quad (11)$$

$$Al(OH)_{3,ads} + OH^- \rightarrow Al(OH)_4^- + ss \quad (12)$$

where ss is the Al surface site. The diffusion of $Al(OH)_x$ ions plays an important role in anodic dissolution due to the formation of an intermediate layer, and the maximum reaction rate occurs at the limiting current condition [28].

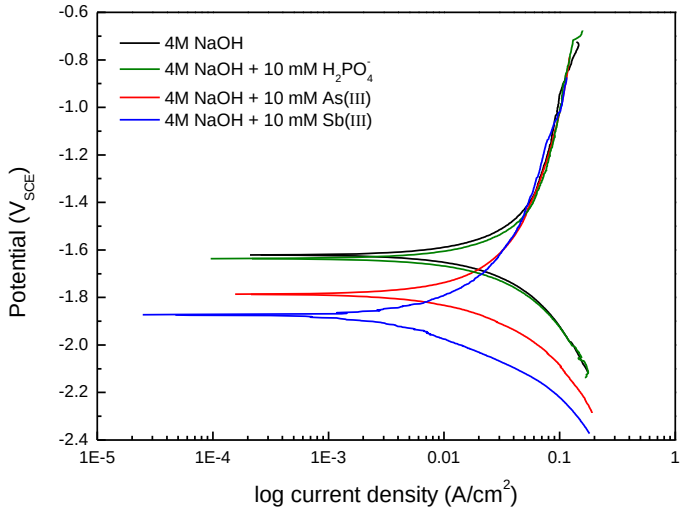

Figure 2. Potentiodynamic polarization curves of 4N Al in 4M NaOH, 4M NaOH + 10 mM As(Ⅲ), 4M NaOH + 10 mM $H_2PO_4^-$, and 4M NaOH + 10 mM Sb(Ⅲ).

Table 3. Electrochemical parameters of the potentiodynamic polarization tests in four electrolytes

Solution	E_{corr} (V_{SCE})	i_{corr} (mA cm^{-2})	β_a ($V\ dec^{-1}$)	β_c ($V\ dec^{-1}$)	Corrosion rate (mm $year^{-1}$)
4M NaOH	-1.621	7.615	0.123	-0.154	83.060
4M NaOH + 10 mM As(Ⅲ)	-1.787	4.258	0.123	-0.123	46.447
4M NaOH + 10 mM $H_2PO_4^-$	-1.637	7.185	0.123	-0.143	78.364
4M NaOH + 10 mM Sb(Ⅲ)	-1.873	2.291	0.124	-0.120	24.989

The anodic reaction curves have similar limiting current densities and similar anodic Tafel slopes in all of the four electrolytes, likely because the additives do not significantly affect dissolution of Al. Simultaneous with the anodic reaction, water reduction occurs [9,27]:

$$ss + H_2O + e^- \rightarrow H_{ads} + OH^- \quad (13)$$

$$H_{ads} + H_2O + e^- \rightarrow H_2 + OH^- + ss \quad (14)$$

In Figure 2, the negative shift of E_{corr} is due to the suppression of the cathodic reaction and/or acceleration of the anodic reaction according to the mixed-potential theory [24,29]. If the anodic reaction is accelerated, the corrosion current density is increased, but the suppressed cathodic reaction induces a decrease of corrosion current density. Thus, it is considered that the additives (As(Ⅲ), $H_2PO_4^-$, Sb(Ⅲ)) act as the cathodic inhibitor that suppresses the cathodic reaction, thereby decreasing the corrosion rate. Also, the cathodic Tafel slopes are lower as the additives are added, which means that the corrosion rate decreases by suppressing the cathodic reaction [20]. Consequently, this

phenomenon indicates that the inhibition of hydrogen evolution by the additives reduces the self-corrosion of 4N Al. The efficiency of the Al-air battery can therefore be improved by suppressing the cathodic reaction [30,31].

Figure 3 shows Nyquist plots for 4N Al in 4M NaOH and experimental group electrolytes under the OCP condition. The impedance spectra appear in three loops, and the equivalent electrical circuits for each electrolyte are represented in Figure 4. The three loops are explained as follows: (i) a first capacitance loop in the high frequency region indicates the redox Al-Al^+ reaction, (ii) an inductance loop in the middle frequency region is due to the adsorption of intermediates such as $Al(OH)_x$ on the Al surface in the Al dissolution process, and (iii) a second capacitance loop in the low frequency region is attributed to the redox Al^+-Al^{3+} reaction. The equivalent circuit consists of the following elements: R_s represents the solution resistance, CPE1 is the capacitance generated by Al dissolution reaction and the electric double layer, and R_{ct} is the charge-transfer resistance between Al and electrolyte interface. The CPE1 and R_{ct} connected in parallel are related to reaction (i). The inductance L and the resistance R_1 of the adsorbed layer are connected in parallel, and these elements are associated with reaction (ii). CPE2 is the dielectric strength of the intermediate layer and water adsorbed on it, and R_2 represents the electrical resistance of the ionic conduction path formed by pores of the intermediate layer. CPE2 and R_2 are the elements corresponding to reaction (iii). The constant phase element (CPE) contains not only a double layer capacitance but also a phenomenological coefficient (n), and is described as:

$$Z_{CPE} = 1/[Q(j\omega)^n] \quad (15)$$

where Q is a proportionality coefficient, j is an imaginary number, ω is the sine wave modulation angular frequency, and n is an empirical exponent that describe the deviation from the ideal capacitance behavior [6,32].

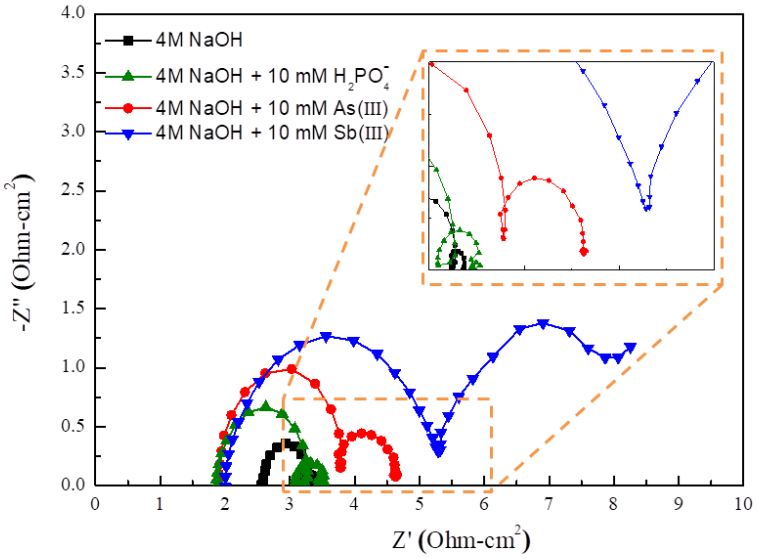

Figure 3. Nyquist plots of 4N Al in 4M NaOH electrolytes containing different additives (As(Ⅲ), $H_2PO_4^-$, Sb(Ⅲ)).

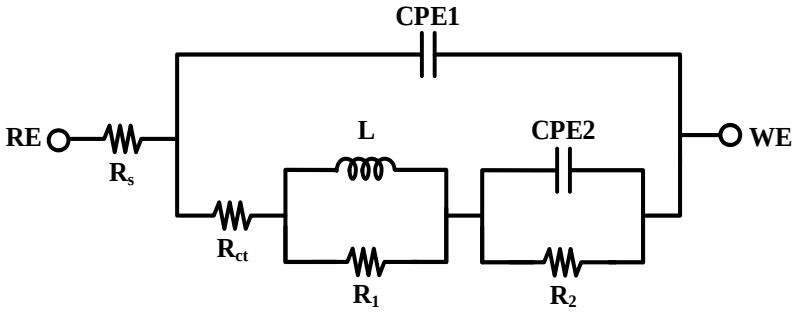

Figure 4. Equivalent circuit model for interpretation of the impedance spectra for 4N Al in 4M NaOH, 4M NaOH + 10 mM As(Ⅲ), 4M NaOH + 10 mM $H_2PO_4^-$ and 4M NaOH + 10 mM Sb(Ⅲ).

Table 4 lists the fitted EIS data from the circuit of the four electrolytes. Optimized values were obtained using the ZSimpwin program. The polarization resistance, R_p, indicates the polarization resistance and is the sum of R_{ct}, R_1 and R_2, the total resistance of the electrochemical reaction of Al in each electrolyte. The values of R_{ct}, R_1, R_2 and R_p decreased in the following order: 4M NaOH + 10 mM Sb(Ⅲ) > 4M NaOH + 10 mM As(Ⅲ) > 4M NaOH + 10 mM $H_2PO_4^-$ > 4M NaOH, indicating that the addition of additive decreases Al dissolution reaction by self-corrosion. The inductance (L) is related to the relaxation time (τ) for adsorption effect. Thus, if the relaxation time is long because of delayed adsorption, the value of inductance also becomes large [33]. As shown in Figure 3, the electrolyte with Sb(Ⅲ) addition seems to appear no inductance. Because elements L and R_1 indicate the resistance of the adsorbed layer formed by intermediates $Al(OH)_x$, it is believed that Sb(Ⅲ) reacts with the $Al(OH)_x$ and rapidly diffuses into the electrolyte, inhibiting the adsorption of $Al(OH)_x$ onto the Al surface [34]. Thus, the inductance values in 4M NaOH + 10 mM Sb(Ⅲ) are significantly larger than those reported for the other electrolytes, as represented in Table 4.

Table 4. Impedance parameters of 4N Al in four electrolytes: 4M NaOH, 4M NaOH + 10 mM As(Ⅲ), 4M NaOH + 10 mM $H_2PO_4^-$, 4M NaOH + 10 mM Sb(Ⅲ).

Solutions	R_s (Ω-cm^2)	CPE1		R_{ct} (Ω-cm^2)	L (H-cm^2)	R_1 (Ω-cm^2)	CPE2		R_2 (Ω-cm^2)	R_p (Ω-cm^2)
		C_{dl} (F cm^{-2})	n (0-1)				C_2 (F cm^{-2})	n (0-1)		
4M NaOH	2.596	0.09×10^{-3}	1	0.619	5.83×10^{-5}	0.093	9.35×10^{-2}	0.992	0.159	0.872
4M NaOH + 10 mM As(Ⅲ)	1.898	0.12×10^{-3}	1	1.729	71.57×10^{-5}	0.261	4.36×10^{-2}	0.904	1.034	3.024
4M NaOH + 10 mM $H_2PO_4^-$	1.897	0.06×10^{-3}	0.999	1.165	32.68×10^{-5}	0.221	3.71×10^{-2}	1	0.432	1.818
4M NaOH + 10 mM Sb(Ⅲ)	1.975	0.09×10^{-3}	0.860	2.245	494.30×10^{-5}	0.829	5.53×10^{-2}	0.550	5.530	8.604

3.3. Battery performance

To confirm the discharge performance in each of the four electrolytes for Al-air battery, battery performance was tested with two electrodes (4N Al and air electrode). Figure 5 and Table 5 represent the results of discharge potentials at the applied current of 10 mA cm^{-2} for 2 h. In Table 5, each parameter is calculated as follows:

$$\text{Capacity density}, Q\ (mAh/g) = it/\Delta m \quad (16)$$

$$\text{Energy density}, W\ (\text{Wh}/kg) = Q\ (mAh/g) \times V\ (\text{V}) \quad (17)$$

where i is the current density (mA cm^{-2}), t is the time (hour), Δm is the weight loss (g cm^{-2}), and V is the average voltage.

$$\text{Current efficiency}, \rho\ (\%) = (Q/Q_0) \times 100 \quad (18)$$

$$\text{Fuel efficiency}, \omega\ (\%) = (W/W_0) \times 100 \quad (19)$$

where Q_0 is the theoretical capacity density (2980 mAh g^{-1}), and W_0 is the theoretical energy density (8100 Wh kg^{-1}).

As shown in Figure 5 and Table 5, the V, Q, ρ, W and ω of Al-air battery in each electrolyte follow the order: 4M NaOH + 10 mM Sb(Ⅲ) > 4M NaOH + 10 mM As(Ⅲ) > 4M NaOH + 10 mM $H_2PO_4^-$ > 4M NaOH, which means that electrolytes with additives have better discharge battery performance than 4M NaOH. The main reason for the increased efficiency with additives is the decreased self-corrosion reaction by the limitation of hydrogen evolution. Also, although V showed a tendency to decrease while applying current in all electrolytes, the degree of decrease in Sb(Ⅲ)-added electrolyte was not larger than that of the other electrolytes. It is known that the decrease of V is due to the formation of aluminum oxidation product, $Al(OH)_3$, and that this product precipitates on the Al surface during the discharge test, acting as a barrier to ion transfer [6]. As a result, the addition of Sb(Ⅲ) in 4M NaOH not only reduces hydrogen generation but also facilitates the diffusion of Al oxidation product on the Al surface.

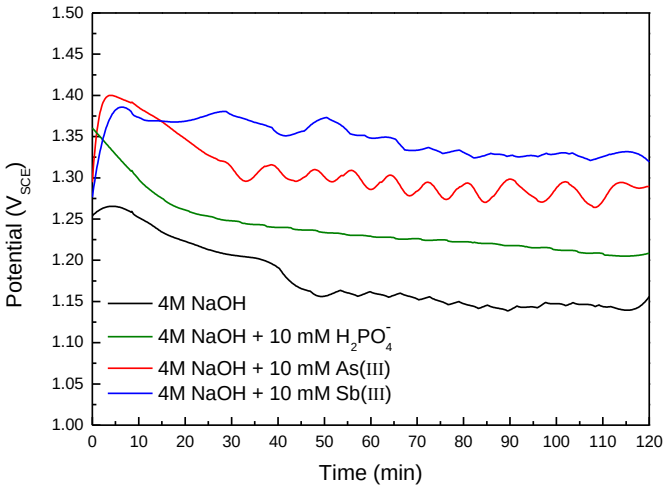

Figure 5. Discharge behavior of Al-air battery based on 4N Al in 4M NaOH electrolyte with and without additives (As(Ⅲ), $H_2PO_4^-$, Sb(Ⅲ)) at 10 mA cm^{-2}.

Table 5. Discharge performance of Al-air battery in four electrolytes at 10 mA cm^{-2}.

Solution	Average discharge voltage, *V* (SCE)	Capacity density *Q* (mAh g^{-1})	Current efficiency ρ (%)	Energy density *W* (Wh kg^{-1})	Fuel efficiency ω (%)
4M NaOH	1.177	702.99	23.590	827.52	10.216
4M NaOH + 10 mM As(Ⅲ)	1.308	1562.50	52.433	2044.40	25.239
4M NaOH + 10 mM $H_2PO_4^-$	1.240	779.73	26.165	966.53	11.932
4M NaOH + 10 mM Sb(Ⅲ)	1.348	1801.80	60.463	2428.67	29.984

To confirm the stability of the air electrode during operation of an Al-air battery, a three-electrode discharge experiment was conducted by adding the SCE electrode. Figure 6 shows the potentials of the 4N Al electrode and the air electrode measured during 10 mA cm^{-2} discharge tests in 4M NaOH, 4M NaOH + 10 mM As(Ⅲ), 4M NaOH + 10 mM $H_2PO_4^-$, and 4M NaOH + 10 mM Sb(Ⅲ) electrolytes. The average potential of the air electrode was not significantly different in any of the electrolytes, but that of the Al electrode differed depending on the electrolyte. Therefore, the extent to which the additives (As(Ⅲ), $H_2PO_4^-$, Sb(Ⅲ)) reacts on the air electrode is insignificant. Also, the cell voltage, the potential difference between 4N Al electrode and air electrode, showed the same tendency as the average voltage *V* in two-electrode discharge tests.

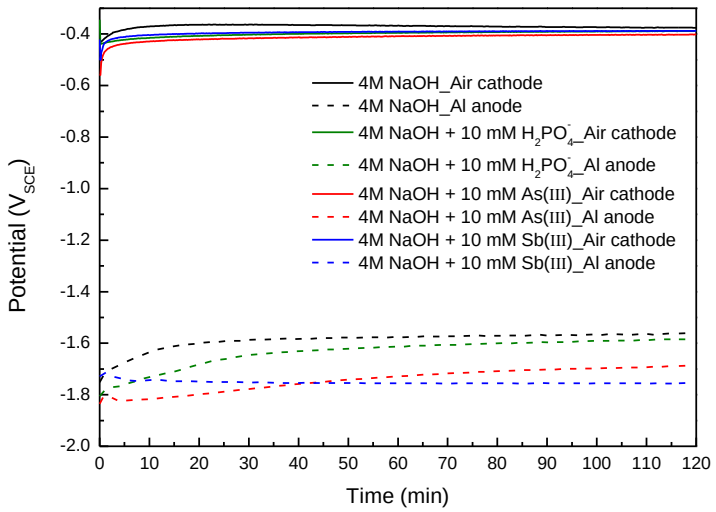

Figure 6. Potential vs time transients of 4N Al and air electrodes during 10 mA cm^{-2} discharge experiment of Al-air battery in four electrolytes.

3.4. Surface analysis

Figure 7 shows the SEM images of 4N Al specimens after 1 h immersion in 4M NaOH, 4M NaOH + 10 mM As(Ⅲ), 4M NaOH + 10 mM $H_2PO_4^-$, and 4M NaOH + 10 mM Sb(Ⅲ) electrolytes. The apparent damage in the SEM image was caused by hydrogen evolution from the Al surface. Decreased damage on the Al surface means, therefore, that hydrogen evolution was suppressed on the surface. The damage of the specimen immersed in the 4M NaOH electrolyte was significantly larger than that of the specimens immersed in the other electrolytes. This is thought to be due to the generation of a large amount of hydrogen on the Al surface in 4M NaOH. The damage formed on the Al specimen in 4M NaOH + 10 mM $H_2PO_4^-$ electrolyte seem to be uniform in size but of greater depth and occurring in larger numbers than those on the specimens from other electrolytes. The damage formed on the specimens from 4M NaOH + 10 mM As(Ⅲ) and 4M NaOH + 10 mM Sb(Ⅲ) electrolytes appeared to be relatively shallow in depth and few in number. As shown in Figure 7, considering the number, size, and depth of the damage, the trend increases in the following order: 4M NaOH + 10 mM Sb(Ⅲ) < 4M NaOH + 10 mM As(Ⅲ) < 4M NaOH + 10 mM $H_2PO_4^-$ < 4M NaOH. This tendency is consistent with the hydrogen evolution rate.

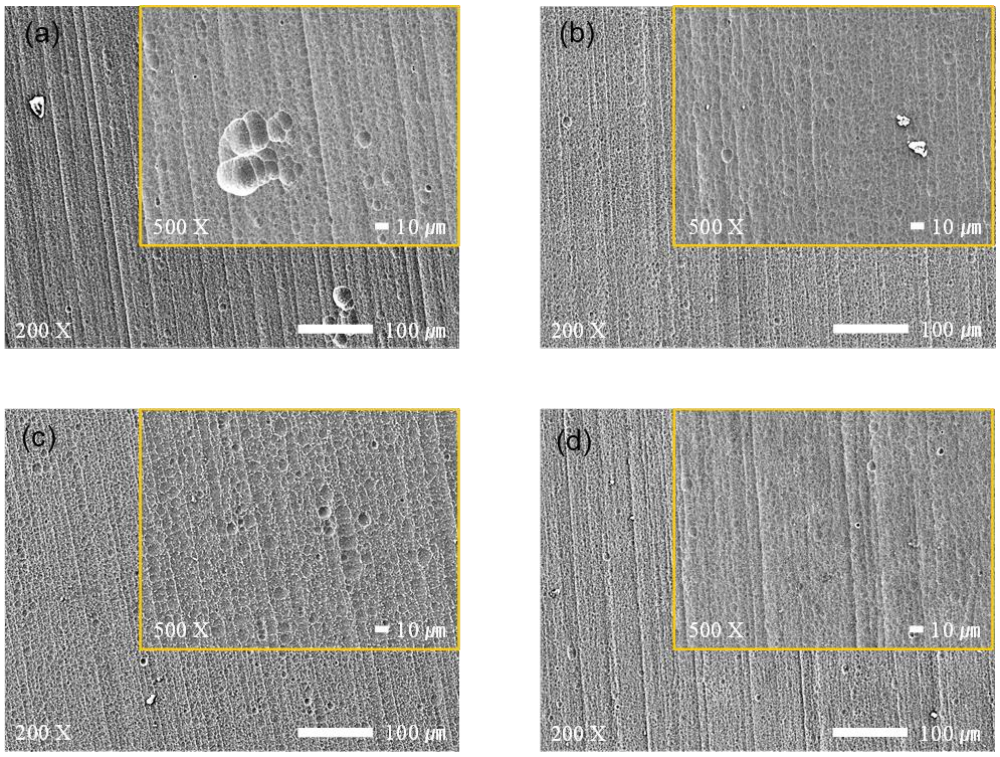

Figure 7. SEM images of 4N Al after 1 h immersion in (a) 4M NaOH, (b) 4M NaOH + 10 mM As(Ⅲ), (c) 4M NaOH + 10 mM $H_2PO_4^-$, and (d) 4M NaOH + 10 mM Sb(Ⅲ)

The additives As(Ⅲ), $H_2PO_4^-$, and Sb(Ⅲ), called poisons, are generally known to retard cathodic reactions of hydrogen on metal [24,35-37]. The hydrogen atom is so small that it can easily migrate through the crystal structure of metal, which has a deleterious effect on the metallurgical and

mechanical properties of the metal [24]. The initial hydrogen enters the metal lattice in an atomic hydrogen state (H) and changes to a hydrogen molecular state (H_2) at the metal surface. The presence of the poisons increases hydrogen damage by delaying the H transformation into H_2 by increasing the activity of H on the surface. The properties of these poisons that play a role in delaying formation of H_2 inhibit the hydrogen evolution reaction which is represented in formula (3). M. Smialowski [38] found that the additive As(Ⅲ) distinctly promotes the penetration of hydrogen into metal cathode which means that the As(Ⅲ) effectively increases the resistance time of H on the metal surface to inhibits the hydrogen evolution reaction in an Al-air battery. However, if P forms $H_2PO_4^-$, it cannot acts as the poison. Thus, the addition of $H_2PO_4^-$ is only slightly effective for inhibition of the hydrogen evolution reaction. Also, the addition of Sb(Ⅲ) inhibits the hydrogen evolution reaction by increasing the overvoltage of hydrogen evolution as a layer forms and adsorbs hydrogen on the cathode surface [39]. Thus, the addition of As(Ⅲ), $H_2PO_4^-$, Sb(Ⅲ) can improve battery performance by suppressing the self-corrosion of Al.

4. CONCLUSIONS

This study investigated the additive effects of arsenic (As(Ⅲ)), phosphorous ($H_2PO_4^-$), and antimony (Sb(Ⅲ)) in 4M NaOH electrolyte for Al-air battery using hydrogen evolution test, self-corrosion test, electrochemical tests, discharge test, and surface analysis. Based on the results, the conclusions are summarized as follows:

(1) Hydrogen evolution and self-corrosion tests revealed that the addition of additives caused the reductions in hydrogen generation and self-corrosion. The slower was the hydrogen evolution rate, the slower was the self-corrosion rate of 4N Al. The trend order is as follows: 4M NaOH + 10 mM Sb(III) < 4M NaOH + 10 mM As(Ⅲ) < 4M NaOH + 10 mM $H_2PO_4^-$ < 4M NaOH.

(2) The As(Ⅲ), $H_2PO_4^-$, and Sb(III) additives shift the open-circuit potentials of 4N Al to negative values and decrease the corrosion rate. This phenomenon is due to the additives acting to suppress the cathodic reaction, which is the hydrogen evolution reaction. Also, the increased polarization resistance in EIS results means that the additives decrease the Al dissolution reaction. Thus, inhibition of hydrogen evolution by the additives reduces the self-corrosion of 4N Al.

(3) The efficiency of an Al-air battery increased with additives without affecting the air electrode. Especially, the addition of Sb(III) to 4M NaOH facilitated the diffusion of $Al(OH)_x$ on the Al surface, resulting in a very large inductance value in EIS.

(4) The SEM results show that the number, size, and depth of the damage tend to decrease with decreased hydrogen evolution reaction.

ACKNOWLEDGEMENT
This work was supported by the National Research Foundation of Korea (NRF) grant funded by the Korea Government (Ministry of Education, Science and Technology) (No. NRF-2019R1A2B5B01070453).

References

1. X. Zhang, X.G. Wang, Z. Xie, Z. Zhou, *Green. Energy Environ*., 1 (2016) 4-17.
2. M.A. Rahman, X. Wang, C. Wen, *J. Electrochem. Soc*., 160 (2013) A1759-A1771.
3. D. Gelman, B. Shvartsev, I. Wallwater, S. Kozokaro, V. Fidelsky, A. Sagy, A. Oz, S. Baltianski, Y. Tsur, Y.E. Eli, *J. Power Sources*, 364 (2017) 110-120.
4. G. Girishkumar, B. McCloskey, A.C. Luntz, S. Swanson, W. Wilcke, *J. Phys. Chem. Lett*., 1 (2010) 2193-2203.
5. Y.J. Cho, I.J. Park, H.J. Lee, J.G. Kim, *J. Power Sources*, 277 (2015) 370-378.
6. I.J. Park, S.R. Choi, J.G. Kim, *J. Power Sources*, 357 (2017) 47-55.
7. Q. Li, N.J. Bjerrum, *J. Power Sources*, 110 (2002) 1-10.
8. L. Fan, H. Lu, *J. Power Sources*, 284 (2015) 409-415.
9. D.R. Egan, C. P. León, R.J.K. Wood, R.L. Jones, K.R. Stokes, F.C. Walsh, *J. Power Sources*, 236 (2013) 293-310.
10. M. Mokhtar, M.Z.M. Talib, E.H. Majlan, S.M. Tasirin, W.M.F.W. Ramli, W.R.W. Daud, J. Sahari , *J. Ind. Eng. Chem*., 32 (2015) 1-20.
11. A.A. Mohamad, *Corros. Sci*., 50 (2008) 3475-3479.
12. Y. Liu, Q. Sun, W. Li, K.R. Adair, J. Li, X. Sun, *Green. Energy Environ*., 2 (2017) 246-277.
13. M.A. Streicher, *J. Electrochem. Soc*., 96 (1949) 170-194.
14. R.D. Armstrong, V.J. Braham, *Corros. Sci*., 38 (1996) 1463-1471.
15. R.N. Mutlu, S. Ateş, B.Yazıcı, *Int. J. Hydrogen Energy*, 42 (2017) 23315-23325.
16. Ö. Aslanbas, Y.E. Durmu, H. Tempel, F. Hause, Y.E. Eli, R.A. Eichel, H. Kungl, *Electrochim. Acta*, 276 (2018) 399-411.
17. J. Liu, D. Wan, D. Zhang, L. Gao, T. Lin, *J. Power Sources*, 335 (2016) 1-11.
18. M.A. Deyab, *Electrochim. Acta*, 244 (2017) 178-183.
19. C.D.S. Tuck, J.A. Hunter, G.M. Scamans, *J. Electrochem. Soc*., 134 (1987) 2970-2981.
20. D. Wang, H. Li, J. Liu, D. Zhang, L. Gao, L. Tong, *J. Power Sources*, 293 (2015) 484-491.
21. D. Wang, D. Zhang, K. Lee, L. Gao, *J. Power Sources*, 297 (2015) 464-471.
22. V.S. Sastri, E. Ghali, M. Elboujdaini, John Wiley & Sons, NJ, 2007.
23. Y. Nie. J. Gao, E. Wang, L. Jiang, L.An, X. Wang, *Electrochim. Acta*, 248 (2017) 478-485.
24. D. A. Jones, Principles and prevention of corrosion, Prentice Hall (2011) Upper saddle river, USA.
25. Z. Sun, H. Lu, *J. Electrochem. Soc*., 162 (2015) A1617-A1623.
26. H.J. Lee, I.J. Park, S.R. Choi, J.G. Kim, *J. Electrochem. Soc*., 164 (2017) A549-A554.
27. M.L. Doche, J.J. Rameau, R. Durand, F.N. Cattin, *Corros. Sci*., 41 (1999) 805-826.
28. D. Wang, L. Gao, D. Zhang, D. Yang, H. Wang, T. Lin, *Mater. Chem. Phys*., 169 (2016) 142-151.
29. M.J. Kim, S.H. Lee, J.G. Kim, J.B. Yoon, *Corrosion*, 66 (2010) 125005-125005-9.
30. M. Pino, C. Cuadrado, J. Chaco´n, P. Rodrı´guez, E. Fata´s, P. Oco´n, *J. Appl. Electrochem*., 44 (2 014) 1371-1380.
31. D.D. Macdonald, K.H. Lee, A. Moccari, D. Harrington, *Corrosion*, 44 (1988) 652-657.
32. S.J. Song, J.G. Kim, *Materials*, 11 (2018) 162.
33. A.M. Abdel-Gaber, E. Khamis, H. Abo-Eldahab, S. Adeel, *Mater. Chem. Phys*., 124 (2010) 773-7 79.
34. Q. Wang, H. Miao, Y. Xue, S. Sun, S. Li, Z. Liu, *RSC Adv*., 7 (2017) 25838-25847.
35. T. Zakroczymski, Z.S. Śmiałowska, M. Smialowski, *Mater. Corros*., 26 (1975) 617-624.
36. R.D. McCright, R.W. Staehle, *J. Electrochem. Soc*., 121 (1974) 609-618.
37. B. Cottis, M. Graham, R. Lindsay, S. Lyon, T. Richardson, D. Scantlebury, H. Stott, Elsevier, AM S, 2010.
38. M. Smialowski, Effect of Hydrogen on Iron and Steel During Production, Fabrication, and Use, Pergamon Press, (1962) Oxford, UK

39. Z. Ahmad Principles of Corrosion Engineering and Corrosion Control, Butterworth-Heinemann, (2006) Oxford, UK